Available online at www.sciencedirect.com

ScienceDirect

Advances in Space Research 55 (2015) 2256–2267

ADVANCES IN SPACE RESEARCH (a COSPAR publication)

www.elsevier.com/locate/asr

An LS-MARS method for modeling regional 3D ionospheric electron density based on GPS data and IRI

Szu-Pyng Kao [a,1], Yao-Chung Chen [a,b,*], Fang-Shii Ning [b,2], Yuh-Min Tu [a,1]

[a] National Chung Hsing University, No. 250, Guoguang Rd., South Dist., Taichung City 402, Taiwan, ROC
[b] National Cheng Chi University, No. 64, Sec. 2, Zhinan Rd., Wenshan Dist., Taipei City 116, Taiwan, ROC

Received 24 February 2014; received in revised form 11 January 2015; accepted 3 February 2015
Available online 11 February 2015

Abstract

The methods of developing an accurate and effective ionospheric electron density (IED) model have greatly interested ionosphere researchers. Numerous scholars have proposed many effective and reliable models and methods of global positioning system (GPS)-based computerized ionospheric tomography (CIT) in the past decades. This study introduced a new function-based CIT method, namely the LS-MARS (Least Squares method-Multivariate Adaptive Regression Splines), combining MARS with IEDs calculated by International Reference Ionosphere (IRI) to automatically choose the best representing basis functions for the three-dimensional (3D) electron density inside that modeling area. This selected basis functions was substituted into the observation equation of the GPS total electron content (TEC) to calculate the design matrix. Finally, the weighted damped least squares (WDLS) were adopted to reestimate the IED model coefficients. In contrast to common function-based CIT methods, the LS-MARS can be used to attain optimal 3D model automatically, flexibly, adaptively based on the IRI without a priori knowledge of the IED distribution mathematical function. The findings indicated that the LS-MARS model had a smaller recovery TEC error than did the MARS_IRI2012 model, and the VTEC calculated using the LS-MARS model was closer to the VTEC obtained from International GNSS Service (IGS) final IONEX files than was the VTEC calculated using the MARS_IRI2012 and IRI2012. Therefore, this method exhibits strong modeling effectiveness and reliability, and can be an efficient alternative method for estimating regional 3D IED models.

Keywords: Ionospheric electron density (IED); Function-based; Computerized ionospheric tomography (CIT); LS-MARS; Weighted damped least squares (WDLS)

1. Introduction

The ionosphere is a part of the Earth's upper atmosphere where the free electron density is high enough to disturb the transmission of electromagnetic waves. In the absence of selective availability (SA), the ionosphere can be the largest source of error in GPS navigation and positioning. Ionospheric delay decreases the accuracy of navigation and positioning systems, causing inaccuracies ranging from several to dozens of meters. During severe ionospheric storms, these inaccuracies can exceed hundreds of meters. The keypoint in correcting electromagnetic measurements for ionospheric disturbances is the knowledge of the electron density. The precise ionospheric electron density model is also applicable to space weather studies and geoscience. In recent years the GPS, have become a

* Corresponding author at: National Chung Hsing University, No. 250, Guoguang Rd., South Dist., Taichung City 402, Taiwan, ROC. Tel./fax: +886 422858180.
E-mail addresses: spkao@dragon.nchu.edu.tw (S.-P. Kao), seven680007@gmail.com (Y.-C. Chen), fsn@nccu.edu.tw (F.-S. Ning), tuyuhmin@gmail.com (Y.-M. Tu).
[1] Tel./fax: +886 422858180.
[2] Tel.: +886 2939309x50741; fax: +886 229390251.

http://dx.doi.org/10.1016/j.asr.2015.02.006
0273-1177/

promising tool and been widely used to monitor electron distribution within the ionosphere. Because the scientists can use dual-frequency GPS observations to estimate the total electron content (TEC) and the electron density in the ionosphere. Moreover, the GPS satellites, being in high altitude orbits, are very useful for studying the structure of the entire ionosphere, and GPS is a low-cost, all-weather, near real time and high-resolution atmospheric sounding technique.

Computerized ionospheric tomography (CIT) technology uses radio wave signals emitted by satellites to invert IED models. The concept of CIT was first introduced to the fields of ionosphere by Austen et al. (1986). At that time, the experiments involved using multiple ground stations in the Naval Navigation Satellite System to detect the TEC during radio wave transmissions; subsequently, tomography was used to invert the TEC to produce 2D IED distributions (Austen et al., 1988). As GPS and GLONASS systems matured and the number of CORS increased, they produced sufficient observation data within a short time, enabling the inversion of IED structures possible; consequently, numerous scholars have proposed effective and reliable CIT methods. Generally, these methods can be divided into function-based and pixel-based methods; Yao et al. (2013) thoroughly described the developmental history and characteristics of these methods. The function-based method is based on the concept that during the model construction process, the IED distribution can be described using mathematical functions such as spherical harmonics combined with empirical orthogonal functions (Fremouw et al., 1992; Gao and Liu, 2002; Hansen, 1998; Howe, 1997; Liu, 2004), or empirical orthogonal function integrated with the Chapman profile (Brunini et al., 2004) or a B-spline (Schmidt et al., 2008; Zeilhofer et al., 2009). The primary purpose of the function-based method is to estimate the function coefficient. By contrast, the pixel-based is based on the concept of dividing the modeling regions into equally sized pixels and assuming that the pixel points for identical pixels possess identically sized IEDs before using an inversion technique to estimate the IED (An, 2011; Hernandez-Pajares et al., 1999; Kamp, 2013; Kunitake et al., 1995; Ma and Maruyama, 2003; Rius et al., 1997; Wen, 2007; Wen et al., 2012; Zou, 2004; Zou and Xu, 2003).

The keypoint to the function-based method is selecting an optimal mathematical function to represent the spatial–temporal distribution of the IEDs in the modeling area during model construction, and subsequently using the inversion theory to effectively estimate the function coefficient. But researchers have experienced difficulties in choosing ionospheric mathematical functions and parameters. Therefore, developing a new modeling method that can automatically, flexibly, and adaptably generate a mathematical function should considerably enhance the effectiveness and convenience of the function-based method. Based on the mentioned assertions, this study proposed a novel CIT method called the Least Squares method-Multivariate Adaptive Regression Splines (LS-MARS). The IEDs calculated by International Reference Ionosphere (IRI) in the modeling area were used as the training data and the MARS statistical learning technique was used to choose the best representing basis functions for the electron density. Subsequently, the selected basis functions was substituted into the observation equation of the GPS TEC to calculate the design matrix. Finally, the weighted damped least squares (WDLS) were employed to reestimate the coefficients of the selected basis functions. In contrast to the traditional function-based CIT method, the LS-MARS method features some advantages, such as that it can automatically, accurately, flexibly, and adaptably produce an 3D model based on the IRI values without a priori knowledge of the IED distribution mathematical function. MARS is a statistical learning technique that can be used for models containing high-dimensional data; thus, the LS-MARS is capable of establishing high-dimensional models, thereby contributing to ionosphere research and facilitating model construction. Durmaz et al. (2010) used the MARS technique for VTEC (Vertical Total Electron Content) estimation over the European region. They showed that the algorithm has the ability to efficiently model the regional distribution of the VTEC and MARS can provide similar RMSE values with a much smaller number of coefficients compared to the spherical harmonic modeling. Similar to the LS-MARS concept, the regional 2D ionospheric VTEC model-construction method has been described in a previous study (Kao et al., 2014).

The structure of this paper is as follows: Section 2 describes the methods of preprocessing the observation data obtained from the ground GPS reference stations and how the observation equation was formed. Section 3 introduces the theoretical basis of MARS and describes how the LS-MARS method to model regional 3D ionospheric electron density based on GPS data and IRI. Section 4 details the research data sources and model specifications during estimation, presenting an analysis and comparison of the research findings. Section 5 concludes the paper.

2. GPS observation and preprocessing

GPS is extensively used in various domains such as surveying, geoscience, and navigation. Almost every country has a ground GPS network. The IGS provides researchers with global observation data free of charge. Nowadays the GPS, have become a promising tool and been widely used to monitor electron distribution within the ionosphere. In this study, a geometry-free linear combination of dual-frequency observations was used to estimate the IED. The geometry-free linear combination can completely eliminate the frequency independent terms in the original observation equation, such as the geometrical distance, tropospheric delays, satellite clock error, and receiver clock error, leaving only the differential code bias (DCB) of the satellite (SDCB) and receiver (RDCB) and the difference

between ionospheric delays on L1 and L2 frequencies and noise. GPS pseudo range observations are less accurate compared with carrier phase observations, but the ambiguity must be estimated when using carrier phase observations. To overcome this problem, phase-smoothed code was used to compose geometry-free linear combination of the observations (Schaer, 1999), as follows:

$$\tilde{P}_1(t) = \Phi_1(t) + \bar{P}_1 - \bar{\Phi}_1 + 2 \bullet \frac{f_2^2}{f_1^2 - f_2^2} \bullet ((\Phi_1(t) - \bar{\Phi}_1) - (\Phi_2(t) - \bar{\Phi}_2)) \quad (1)$$

$$\tilde{P}_2(t) = \Phi_2(t) + \bar{P}_2 - \bar{\Phi}_2 + 2 \bullet \frac{f_1^2}{f_1^2 - f_2^2} \bullet ((\Phi_1(t) - \bar{\Phi}_1) - (\Phi_2(t) - \bar{\Phi}_2)) \quad (2)$$

$$\tilde{L}4 = \tilde{P}_1 - \tilde{P}_2 = RDCB + (dion\ 1 - dion\ 2) + SDCB + e \quad (3)$$

where $\tilde{P}_F(t)$ is the smoothed code measurement of frequency F at epoch t; $\Phi_F(t)$ is the carrier phase measurement of frequency F at epoch t; f_F is the frequency of carrier L_F, $f_1 = 1575.42$ MHz, $f_2 = 1227.60$ MHz; $\bar{P}_F - \bar{\Phi}_F$ is the mean difference between all accepted code and phase measurements in the current observation arc on frequency F; and $\tilde{L}4$ is the smoothed geometry-free linear combination in units of meters. *RDCB* and *SDCB* are the differential code bias of the receiver and satellite respectively, in units of meters; *dion1* and *dion2* are the ionospheric delays on L1 and L2, respectively, in units of meters. e is the observation error. Only the first order of ionospheric refraction is considered when estimating the ionospheric delays in GPS processing, because the first order effects account for 99.9% of total. Its conversion relation to the total electron content (TEC) is as follows (Hofmann-Wellenhof et al., 2007):

$$dionF = \frac{40.3}{f_F^2} TEC \quad \text{with} \quad TEC = \int N_e(\phi, \lambda, H) ds \quad (4)$$

where *TEC* is the total electron content of the satellite and receiver ray path, which is typically represented in total electron content units (TECU; 1 TECU $= 10^{16}$ electrons/m^2), and $N_e(\varphi, \lambda, H)$ is the IED at the geographic position of (φ, λ, H). Eq. (4) can be substituted into Eq. (3) to obtain the following:

$$\tilde{L}4 = RDCB + SDCB + 40.3\left(\frac{1}{f_1^2} - \frac{1}{f_2^2}\right) \times \int N_e(\phi, \lambda, H) ds + e \quad (5)$$

3. Methodology

3.1. Multivariate Adaptive Regression Splines

MARS is an adaptive regression procedure from the statistical learning field that was proposed by Friedman (1991). MARS can be considered an extension of linear models that automatically models nonlinearity and the interactions among variables. It is defined as a multivariate, piecewise regression method that can be used to model complex relations between inputs and outputs (Hastie et al., 2009). This piecewise regression method first divides the input space, which is defined as the collection of observation locations, into sub spaces for multiple knots and then fits a spline function between these knots, adaptively using so-called basis functions. In this study the piecewise-cubic type of modeling was employed for building MARS models using ARESLab toolbox (Jekabsons, 2010). The cubic function is given as follows (Friedman, 1991):

$$C(X_j|s = +1, t_1, t, t_2) = \begin{cases} 0, & \text{if } X_j \leqslant t_1 \\ \beta_1(X_j - t_1)^2 + \gamma_1(X_j - t_1)^3, & \text{if } t_1 < X_j < t_2 \\ X_j - t, & \text{if } X_j \geqslant t_2 \end{cases}$$
$$C(X_j|s = -1, t_1, t, t_2) = \begin{cases} t - X_j, & \text{if } X_j \leqslant t_1 \\ \beta_2(X_j - t_2)^2 + \gamma_2(X_j - t_2)^3, & \text{if } t_1 < X_j < t_2 \\ 0, & \text{if } X_j \geqslant t_2 \end{cases} \quad (6)$$

$$\text{with} \quad t_1 < t < t_2, \ \text{Setting}$$
$$\beta_1 = (2t_2 + t_1 - 3t)/(t_2 - t_1)^2$$
$$\gamma_1 = (2t - t_2 - t_1)/(t_2 - t_1)^3$$
$$\beta_2 = (3t - 2t_1 - t_2)/(t_1 - t_2)^2 \quad (7)$$
$$\gamma_2 = (t_1 + t_2 - 2t)/(t_1 - t_2)^3$$
$$t \in \{x_{ij}\}; \quad t_1 = (\min(X_j) + t)/2;$$
$$t_2 = (t + \max(X_j))/2,$$
$$i = 1, 2, \ldots, N; \ j = 1, 2, \ldots, p$$

where N is the number of observations; p is the dimension of the input space; X_j is the jth component of the input space; $x_{i,j}$ is the observed value of the inputs; t is a univariate knot location from the set $\{x_{ij}\}$, t_1 is a univariate knot location for the additional side knot on the left of the central knot t, t_2 is a univariate knot location for the additional side knot on the right of the central knot t; the quantities s in Eq. (6) take on values ± 1 and indicate the (right/left) sense of the associated cubic function.

The idea of MARS is to form the cubic functions for each input X_j with knots at each observed value x_{ij} of that inputs. Subsequently, the functions from the collected cubic functions or their products were used to build a regression function.

A general MARS model is defined as follows (Friedman, 1991):

$$f(\boldsymbol{X}) = a_0 + \sum_{m=1}^{M} a_m B_m(\boldsymbol{X}) \quad (7)$$

where M is the number of basis functions; a_0 is the intercept; a_m is the coefficient of the basis functions; $B_m(\boldsymbol{X})$ is the basis function obtained by a function from the collected cubic functions or their products, $m = 1, 2, \ldots, M$; $\boldsymbol{X} = [X_1, X_2, \ldots, X_p]^{\mathrm{T}}$ is a p dimensional vector of input variables; and $f(\boldsymbol{X})$ is the regression function constructed using MARS.

The basic MARS concept is to build the model by adding basis functions in the forward stepwise procedure and eliminating the term whose removal causes the smallest increase in residual sum of squares (RSS) (least contribution) from the model during the backward deletion procedure (Friedman, 1991; Hastie et al., 2009). In the forward stage (constructive phase) a large over-fitted model of the form Eq. (8) is built. A generalized cross-validation (GCV) statistic is employed to prune the model to overcome this problem in the backward stage (pruning phase). The GCV is defined as follows (Hastie et al., 2009):

$$GCV(\lambda) = \frac{\sum_{i=1}^{N}\left(y_i - \left(\hat{a}_0 + \sum_{m=1}^{M}\hat{a}_m B_m(\boldsymbol{x}_i)\right)\right)^2}{(1 - \alpha(\lambda)/N)^2} \tag{8}$$

where λ is the tuning parameter; N is the number of observations; M is the number of basis functions; y_i is the ith observation with the corresponding observation location $\boldsymbol{x}_i = [x_{i,1}, x_{i,2}, \ldots, x_{i,p}]^{\mathrm{T}}$, $i = 1, 2, \ldots, N$, p is the dimension; $\hat{a}_0$ is the estimated intercept; $\hat{a}_m$ is the estimated coefficient of the basis functions; $B_m(\boldsymbol{X})$ is the basis function, $m = 1, 2, \ldots, M$; and $\alpha(\lambda)$ is the effective number of parameters in the model, which can be determined using $\alpha(\lambda) = r + ck$, where r is the number of linearly independent basis functions in the model. k is the number of knots selected in the forward process and c is the penalty for selecting knots, which is recommended to be 3 (Hastie et al., 2009). In the backward stage, the model that exhibits the minimal GCV value is selected as the optimal MARS model (the forward and backward stage information is detailed in Durmaz et al., 2010; Friedman, 1991; Hastie et al., 2009 and Jekabsons, 2010).

3.2. LS-MARS algorithm

To obtain the optimal 3D IED approximate model, LS-MARS first divided the ionosphere into voxels (pixels in three dimensions) where the electron density distribution within each voxel is considered to be constant and calculated the geographic latitude φ, geographic longitude λ, and the height H above the Earth of the voxel gridpoints. Fig. 1 depicts the ionospheric CIT and the voxel gridpoints of the ionosphere obtained in the LS-MARS approach. The optimal 3D IED approximate model can be determined by adjusting the model, using adaptive continuous learning and $\boldsymbol{X} = [\varphi, \lambda, H]^{\mathrm{T}}$ of the voxel gridpoints as the independent variables and the IED values of voxel gridpoints calculated from IRI at the modeling time T as the dependent variable; the MARS algorithm can be employed. The estimated IED model as Eq. (8) form:

$$N_{e\_mars}(\boldsymbol{X}) = \hat{a}_0 + \sum_{m=1}^{M}\hat{a}_m B_m(\boldsymbol{X}) + e \tag{9}$$

where $N_{e\_mars}(\boldsymbol{X})$ is the IED approximate model; $\hat{a}_0$ is the estimated intercept; $\hat{a}_m$ is the estimated coefficient of the basis functions; and $B_m(\boldsymbol{X})$ is the selected basis function by MARS to fit IRI, $m = 1, 2, \ldots, M$; e is the observation error.

In this study, we focus on the estimation of IED; thus, the DCB values for the satellites and receivers are obtained from IGS Final IONEX files through the Internet and substituted in Eq. (5) for SDCB and RDCB parts to derive TEC as:

$$Y = \frac{\tilde{L}4 - SDCB - RDCB}{40.3(1/f_1^2 - 1/f_2^2)} = \int_{\mathrm{Pr}}^{Ps} N_e(\boldsymbol{X})ds + e \tag{10}$$

where Y is the TEC observation; $\boldsymbol{X}$ is the observation location; e is the observation error; Ps and Pr are the upper and lower integral bounds, are defined as the points where the ray-path of a GPS signal intersects the upper and lower ionosphere, respectively see Fig. 1.

The selected basis functions from $N_{e\_mars}(\boldsymbol{X})$ are substituted into Eq. (11), yielding the following observation equation:

$$Y = \int_{\mathrm{Pr}}^{Ps}\left[a_0 + \sum_{m=1}^{M}a_m B_m(\boldsymbol{X})\right]ds + e \tag{11}$$

Eq. (12) is the fundamental observation equation for conducting 3D IED modeling by using tomographic inversion based on GPS data and IRI by using LS-MARS. If there are N observations, the observation equations can be expressed as follows:

$$\overbrace{\begin{bmatrix} y_1 \\ y_2 \\ \vdots \\ y_N \end{bmatrix}}^{Y}_{N\times 1} = \overbrace{\begin{bmatrix} DS(1) & \int_{\mathrm{Pr}(1)}^{Ps(1)} B_1(\boldsymbol{X})ds & \int_{\mathrm{Pr}(1)}^{Ps(1)} B_2(\boldsymbol{X})ds & \cdots & \int_{\mathrm{Pr}(1)}^{Ps(1)} B_M(\boldsymbol{X})ds \\ DS(2) & \int_{\mathrm{Pr}(2)}^{Ps(2)} B_1(\boldsymbol{X})ds & \int_{\mathrm{Pr}(2)}^{Ps(2)} B_2(\boldsymbol{X})ds & \cdots & \int_{\mathrm{Pr}(2)}^{Ps(2)} B_M(\boldsymbol{X})ds \\ \vdots & \vdots & \vdots & \cdots & \vdots \\ DS(N) & \int_{\mathrm{Pr}(N)}^{Ps(N)} B_1(\boldsymbol{X})ds & \int_{\mathrm{Pr}(N)}^{Ps(N)} B_2(\boldsymbol{X})ds & \cdots & \int_{\mathrm{Pr}(N)}^{Ps(N)} B_M(\boldsymbol{X})ds \end{bmatrix}}^{A}_{N\times(1+M)} \overbrace{\begin{bmatrix} a_0 \\ a_1 \\ \vdots \\ a_M \end{bmatrix}}^{\Lambda}_{(1+M)\times 1} + \overbrace{\begin{bmatrix} e_1 \\ e_2 \\ \vdots \\ e_N \end{bmatrix}}^{e}_{N\times 1} \tag{12}$$

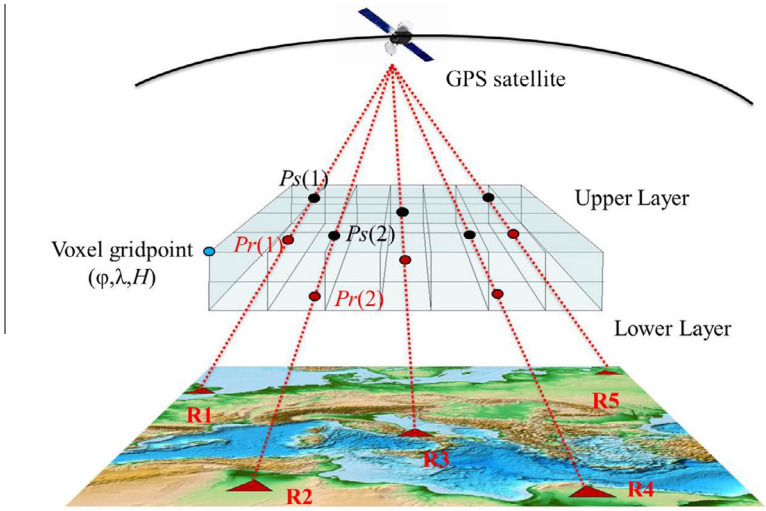

- *Ps*(i), the intersection point of the Ray-path of a GPS signal through the upper-layer ionosphere, i=1,…,5.
- *Pr*(i), the intersection point of the Ray-path of a GPS signal through the lower-layer ionosphere, i=1,…,5.
- The voxel gridpoint of the ionosphere for training MARS model based IRI2012.

Fig. 1. The ionospheric CIT and the voxel gridpoints of ionosphere in LS-MARS approach.

where N is the number of TEC observations; M is the number of basis functions; $\boldsymbol{Y}$ is the $N \times 1$ vector of TEC observations; $\boldsymbol{A}$ is the $N \times (1+M)$ design matrix; $\boldsymbol{\Delta}$ is the $(1+M) \times 1$ vector of unknown parameters; $\boldsymbol{e}$ is the $N \times 1$ vector of observation errors; $DS(i)$ is the ray-path distance from $Ps(i)$ to $Pr(i)$, $\int_{\mathrm{Pr}(i)}^{Ps(i)} B_m(\boldsymbol{X})ds$ is the integral value calculated from mth basis function of the ith observation, $Ps(i)$ and $Pr(i)$ are the upper and lower integral bounds, $i = 1,2,\ldots,N$, $m = 1,2,\ldots,M$; and a_k is the IED model coefficient of MARS that must be reestimated, $k = 0,1,\ldots,M$. In this step, the parametrization and Gauss–Legendre quadrature (Zeilhofer et al., 2009) were applied when the $\boldsymbol{A}$ matrix was calculated.

In this study, it was assumed that the mean and RMS of the observation errors were zero and elevation dependent (Schaer, 1999), respectively. The observation errors were uncorrelated with each other. The variance–covariance matrix and weight matrix for the observations were defined as follows:

$$\boldsymbol{Q} = \begin{bmatrix} \sigma_1^2 & 0 & \cdots & 0 & 0 \\ 0 & \ddots & \cdots & 0 & 0 \\ \vdots & \vdots & \ddots & \vdots & \vdots \\ 0 & 0 & \cdots & \ddots & 0 \\ 0 & 0 & \cdots & 0 & \sigma_N^2 \end{bmatrix}_{N\times N} \quad \text{with} \quad \sigma_i(z_i) = \frac{\sigma_0}{\cos(z_i)} \tag{13}$$

$$\boldsymbol{P} = \sigma_0^2 \boldsymbol{Q}^{-1}$$

where $\boldsymbol{Q}$ is the $N \times N$ diagonal variance–covariance matrix of observations; $\boldsymbol{P}$ is the weight matrix of observations; N is the number of observations; z_i is the zenith angle of the satellite, σ_i is the standard deviation of the observations, $i = 1,2,\ldots,N$; and σ_0 is the standard deviation of unit weight corresponding to an observation at the zenith. The Gauss–Markov model was built using mathematical model Eq. (13) and stochastic model Eq. (14). The key task involved in CIT is estimating the model coefficients as efficiently and accurately as possible by using Eqs. (13) and (14). Unfortunately, the CIT is an under-determined, mixed-determined, ill-posed inverse problem and unknown parameters cannot be reliably or efficiently estimated using the standard least squares inversion technique. To overcome this problem, the so-called weighted damped least squares method was adopted in this study:

$$\hat{\boldsymbol{\Delta}} = \left(\boldsymbol{A}^{\mathrm{T}}\boldsymbol{P}\boldsymbol{A} + \alpha \boldsymbol{P}_{\boldsymbol{X}}\right)^{-1}\left(\boldsymbol{A}^{\mathrm{T}}\boldsymbol{P}\boldsymbol{Y} + \alpha \boldsymbol{P}_{\boldsymbol{X}}\boldsymbol{X}_{\boldsymbol{0}}\right) \tag{14}$$

where α is the regularization parameter; $\boldsymbol{P}_{\boldsymbol{X}}$ and $\boldsymbol{X}_{\boldsymbol{0}}$ are the prior information introduced to stabilize the estimation process, $\boldsymbol{P}_{\boldsymbol{X}}$ is the given weight matrix of unknown parameters and $\boldsymbol{X}_{\boldsymbol{0}}$ is the given initial value of unknown parameters. When solving $\hat{\boldsymbol{\Delta}}$ we may apply the iterative maximum-likelihood variance component estimation to estimate the regularization parameter α see Koch and Kusche (2002). A unit matrix $\boldsymbol{I}$ was introduced to represent the weight matrix of unknown parameters, i.e., supposing that all unknown parameters have the same weights, and the initial value of unknown parameters is $\hat{\boldsymbol{a}} = [\hat{a}_0, \hat{a}_{1,\ldots,}\hat{a}_M]^{\mathrm{T}}$ obtained from Eq. (10).

Finally, the IED model is generated using the selected basis functions from Eq. (10) and the reestimated MARS coefficients from Eq. (15). The calculation was executed using the Matlab program version 7.14.

4. Data and results

The collected GPS data in this study originated from the Western European 42 IGS CORS 24-h dual-frequency GPS observations obtained on February 29 and March 1, 2012 (DoY60–61). The 38 IGS station observations were used to reconstruct the IED model, and observations from the remaining four stations (GRAZ, GRAS, SPT0, and LAMA) were applied to conduct a model quality analysis. To conduct an VTEC verification, the VTEC calculated from the electron density model of LS-MARS was compared with the VTEC obtained from the IGS final IONEX files at A (latitude 55°N, longitude 15°E), B (latitude 45°N, longitude 15°E), and C (latitude 35°N, longitude 15°E) to show the consistency with IGS VTEC maps. Fig. 2 illustrates the distribution of GPS stations and the check points of VTEC verification used in this study. The geographical coverage of the 42 IGS stations is from 0–30° East longitude and 30–60° North latitude. In the region chosen for CIT, the longitude ranged from 0° to 30° East, latitude ranged from 30° to 60° North, and altitude ranged from 100 to 1000 km. The discretized increments in latitude and longitude were 1°, the steps in height were 50 km when the IED values were calculated, using IRI2012 to construct an approximate IED model by using MARS. Thus, 18,259 ($31 \times 31 \times 19$) IEDs of the voxel gridpoints were calculated from IRI2012 to fit the approximate 3D IED model at each epoch. A set of ionospheric electron density coefficients was estimated every 2 h. Table 1 lists the number of GPS signal ray paths and basis functions at every

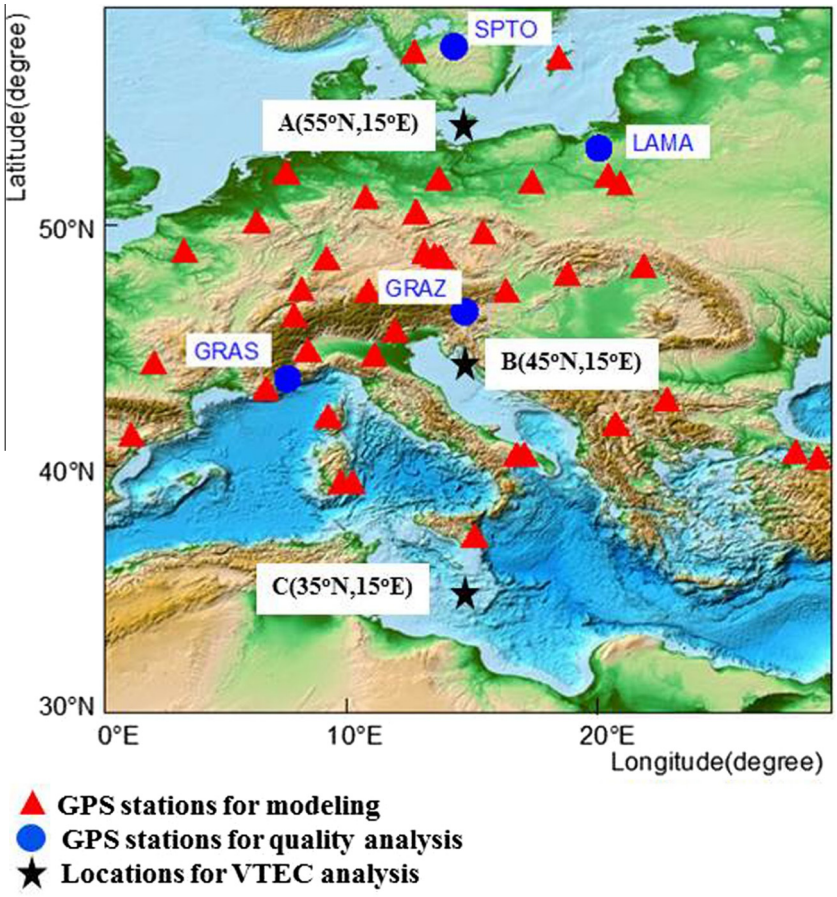

Fig. 2. The distribution of the 42 IGS GPS stations and 3 check points used in this study.

Table 1
The number of GPS signal ray paths (SRP) and basis functions (BF).

		TIME (UT)											
		00:00	02:00	04:00	06:00	08:00	10:00	12:00	14:00	16:00	18:00	20:00	22:00
60	SRP	129	159	236	162	174	198	157	192	184	147	155	177
	BF	45	56	61	48	38	48	30	32	41	50	65	56
61	SRP	117	143	224	149	153	170	135	147	143	138	146	169
	BF	53	59	61	48	37	51	33	36	44	54	65	55

modeling epoch on DoY60 and DoY61 in 2012. When using MARS to train the approximate model, the maximal number of basis functions (including the intercept term) during the forward model building phase (before pruning in the backward phase) was set at 100 and the maximum degree of interaction between input variables (order of products of basis functions allowed) was set to 3; the piecewise-cubic type of modeling was employed.

Fig. 3 shows the TEC measurements from the GPS stations at GRAZ, GRAS, SPTO, and LAMA at every modeling epoch on DoY60 in 2012. Fig. 4 shows the TEC measurements from the GPS stations at GRAZ, GRAS, SPTO, and LAMA at every modeling epoch on DoY61 in 2012. Figs. 5 and 6 show the comparison of the recovery TEC error calculated from LS-MARS and MARS_IRI2012 at GRAZ, GRAS, SPTO, and LAMA at every modeling epoch on DoY60 and DoY61 in 2012, respectively. The MARS_IRI2012 can be considered an approximate model of the IRI2012, which can be estimated using Eq. (10). The recovery TEC error is calculated as follows:

$$R.E = |TEC_{GPS} - TEC_{model}| \tag{15}$$

where TEC_{GPS} are the TEC measurements from the GPS stations at GRAZ, GRAS, SPTO, and LAMA. TEC_{model} are the TEC values derived from the IED model. Fig. 5 indicates that the mean absolute TEC error of the LS-MARS and MARS_IRI2012 are 2.55 TECU and 3.98 TECU, respectively. The RMS of the absolute TEC error of the LS-MARS and MARS_IRI2012 are 3.29 TECU and 5.33 TECU, respectively. Fig. 6 indicates that the mean absolute TEC error of the LS-MARS and MARS_IRI2012 are 2.77 TECU and 3.51 TECU,

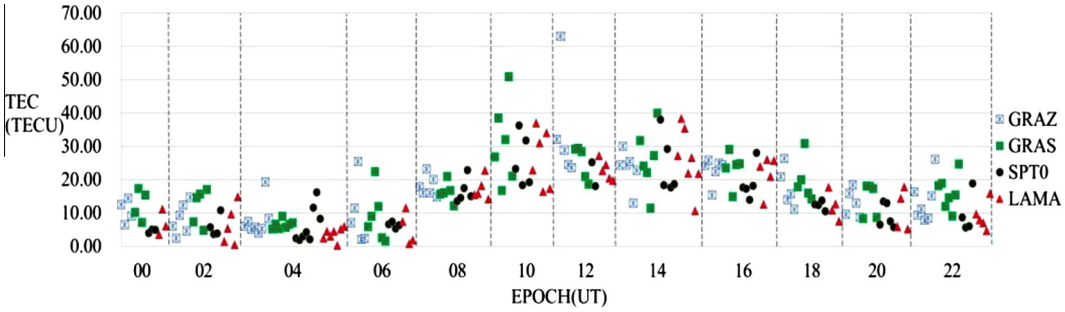

Fig. 3. The TEC measurements from the GPS stations at GRAZ, GRAS, SPTO, and LAMA on DoY60, 2012.

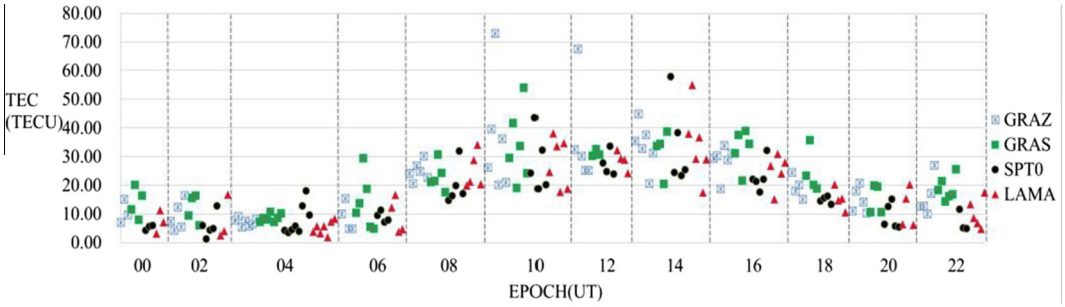

Fig. 4. The TEC measurements from the GPS stations at GRAZ, GRAS, SPTO, and LAMA on DoY61, 2012.

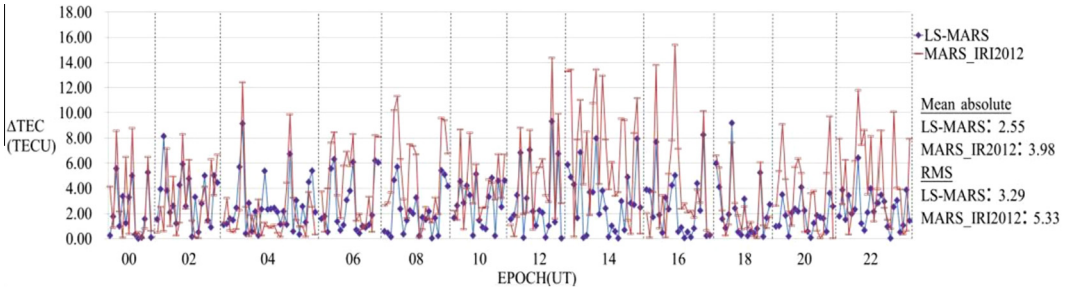

Fig. 5. Comparison of the recovery TEC error calculated from LS-MARS and MARS_IRI2012 at GRAZ, GRAS, SPTO, and LAMA at every modeling epoch on DoY60, 2012.

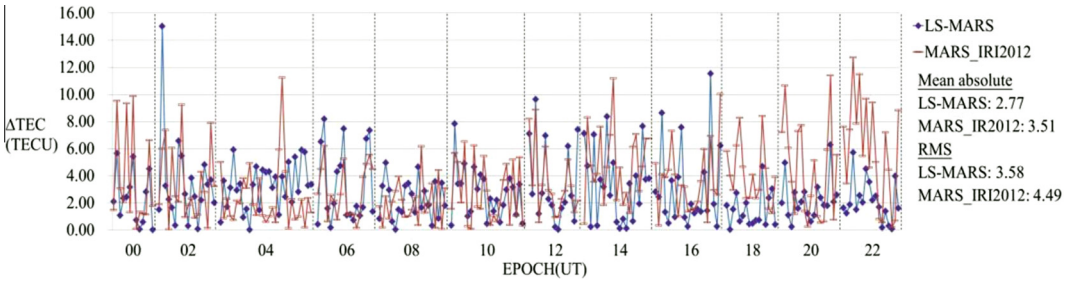

Fig. 6. Comparison of the recovery TEC error calculated from LS-MARS and MARS_IRI2012 at GRAZ, GRAS, SPTO, and LAMA at every modeling epoch on DoY61, 2012.

respectively. The RMS of the absolute TEC error of the LS-MARS and MARS_IRI2012 are 3.58 TECU and 4.49 TECU, respectively. Thus, the results suggest that the LS-MARS model had a smaller recovery TEC error than did the MARS_IRI2012 model.

Table 2
Comparison of the statistical results of absolute ΔVTEC between IGSF and LS-MARS, MARS_IRI2012 and IRI2012 on days from DoY60 to DoY61 in 2012 at A, B and C.

		Absolute ΔVTEC between IGSF and (TECU)		
		LS-MARS	MARS_IRI2012	IRI2012
Mean	A(55°N, 15°E)	0.80	1.76	1.85
	B(45°N, 15°E)	0.72	2.83	2.94
	C(35°N, 15°E)	1.77	2.49	2.58
RMS	A(55°N, 15°E)	0.96	1.97	2.04
	B(45°N, 15°E)	0.85	3.18	3.31
	C(35°N, 15°E)	2.23	3.21	3.27

Table 2 compares the statistical results of absolute ΔVTEC between IGSF and LS-MARS, MARS_IRI2012, and IRI2012 on days from DoY60 to DoY61 during 2012 at A, B, and C. Figs. 7–9 compare the VTEC calculated from LS-MARS, MARS_IRI2012, IRI2012 and IGSF on days from DoY60 to DoY61 in 2012 at A, B and C, respectively. Table 2 indicates that the mean absolute ΔVTEC between IGSF and LS-MARS at A, B and C are 0.80 TECU, 0.72 TECU and 1.77 TECU, respectively. The RMS of absolute ΔVTEC between IGSF and LS-MARS at A, B and C are 0.96 TECU, 0.85 TECU and 2.23 TECU, respectively. The results suggest that the VTEC calculated from LS-MARS was closer to the VTEC

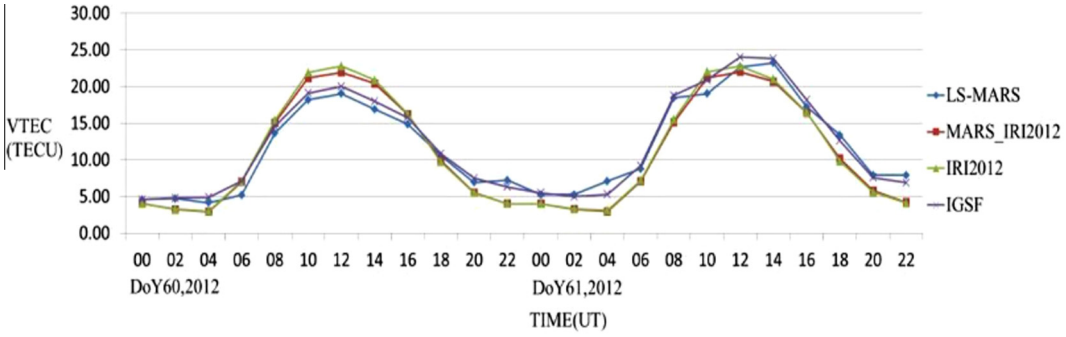

Fig. 7. Comparison of the VTEC calculated from LS-MARS, MARS_IRI2012, IRI2012 and IGSF on days from DoY60 to DoY61 in 2012 at A.

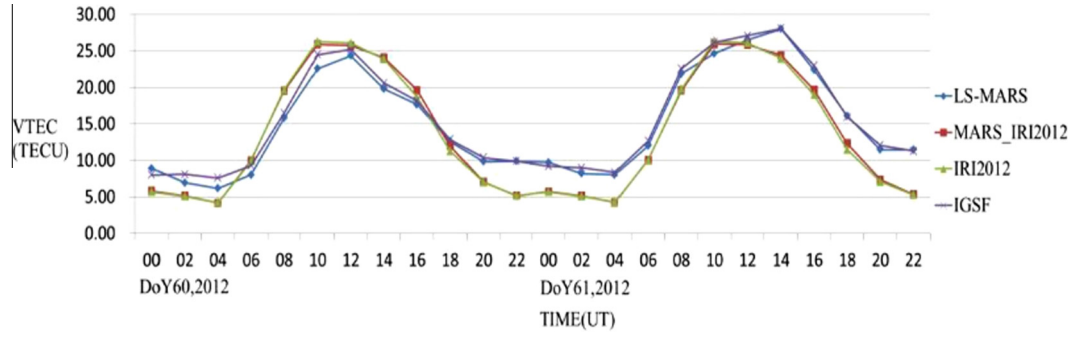

Fig. 8. Comparison of the VTEC calculated from LS-MARS, MARS_IRI2012, IRI2012 and IGSF on days from DoY60 to DoY61 in 2012 at B.

obtained from the IGS final IONEX files than was the VTEC calculated from MARS_IRI2012 and IRI2012. The VTEC calculated from MARS_IRI2012 and IRI2012 were very close.

Figs. 10–15 show the distribution of IED for LS-MARS and the error IED between IRI2012 and LS-MARS at heights of 300, 400, 500 km at UT10:00 on days from DoY60 to DoY61 in 2012, all of their units are 1 el/m^3;

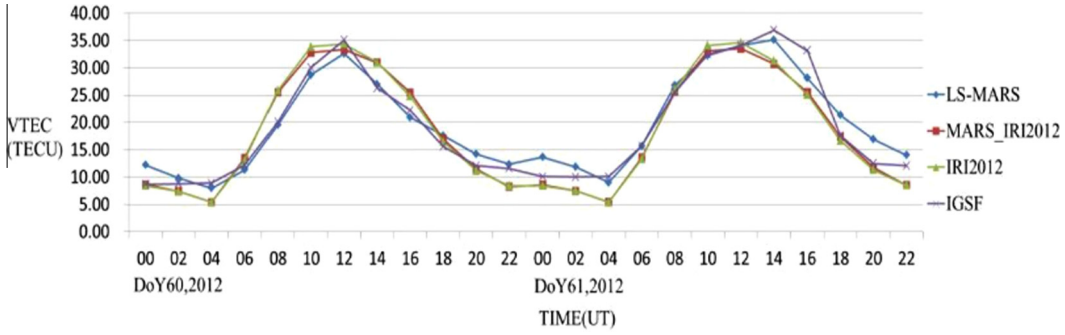

Fig. 9. Comparison of the VTEC calculated from LS-MARS, MARS_IRI2012, IRI2012 and IGSF on days from DoY60 to DoY61 in 2012 at C.

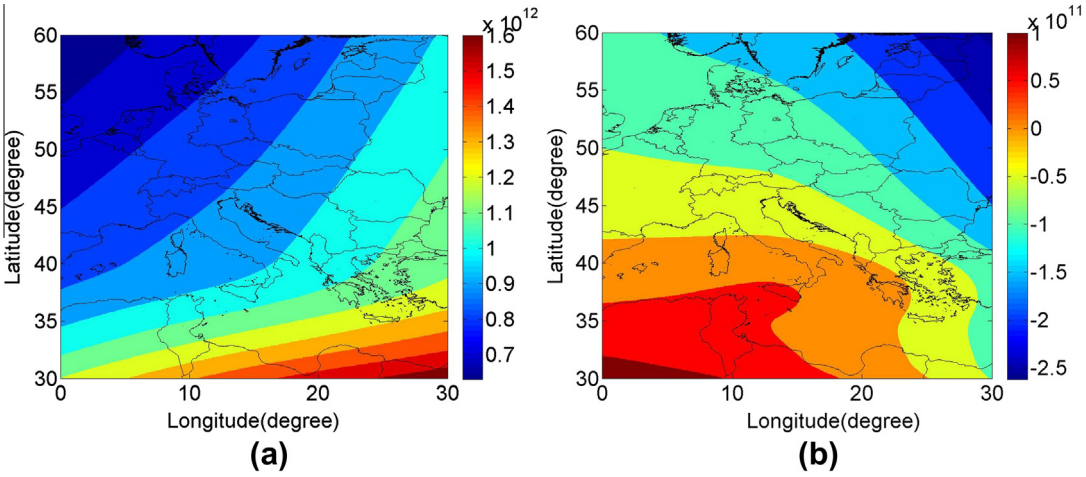

Fig. 10. The distribution of IED for LS-MARS (a) and the error IED between IRI2012 and LS-MARS (b) at heights of 300 km at UT10:00 on DoY60 in 2012, the RMS of the error IED is 9.18E+10 el/m^3.

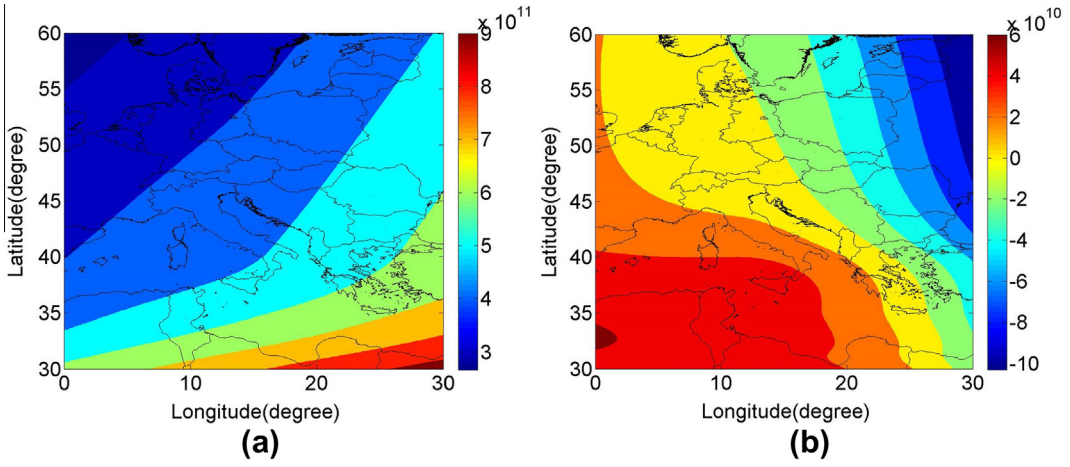

Fig. 11. The distribution of IED for LS-MARS (a) and the error IED between IRI2012 and LS-MARS (b) at heights of 400 km at UT10:00 on DoY60 in 2012, the RMS of the error IED is 3.80E+10 el/m^3.

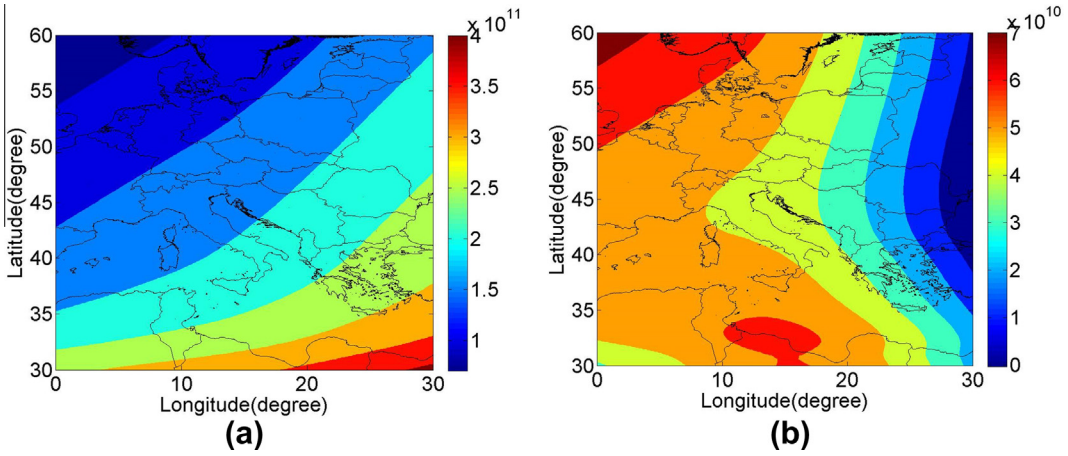

Fig. 12. The distribution of IED for LS-MARS (a) and the error IED between IRI2012 and LS-MARS (b) at heights of 500 km at UT10:00 on DoY60 in 2012, the RMS of the error IED is 4.74E+10 el/m^3.

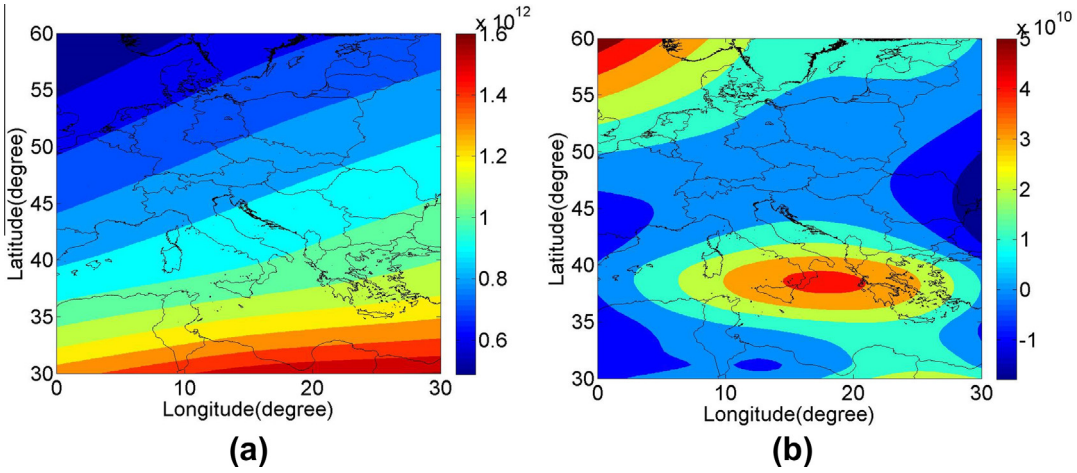

Fig. 13. The distribution of IED for LS-MARS (a) and the error IED between IRI2012 and LS-MARS (b) at heights of 300 km at UT10:00 on DoY61 in 2012, the RMS of the error IED is 2.46E+10 el/m^3.

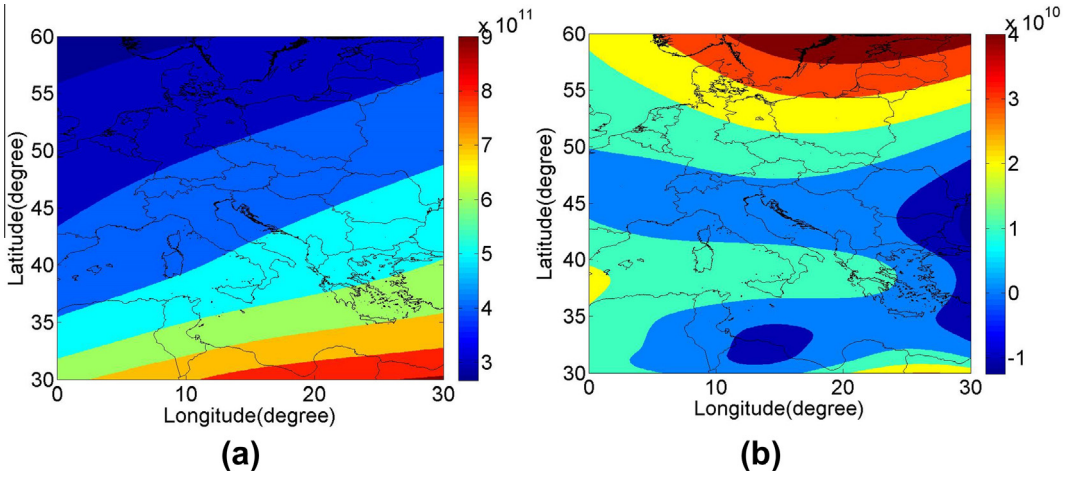

Fig. 14. The distribution of IED for LS-MARS (a) and the error IED between IRI2012 and LS-MARS (b) at heights of 400 km at UT10:00 on DoY61 in 2012, the RMS of the error IED is 4.08E+10 el/m^3.

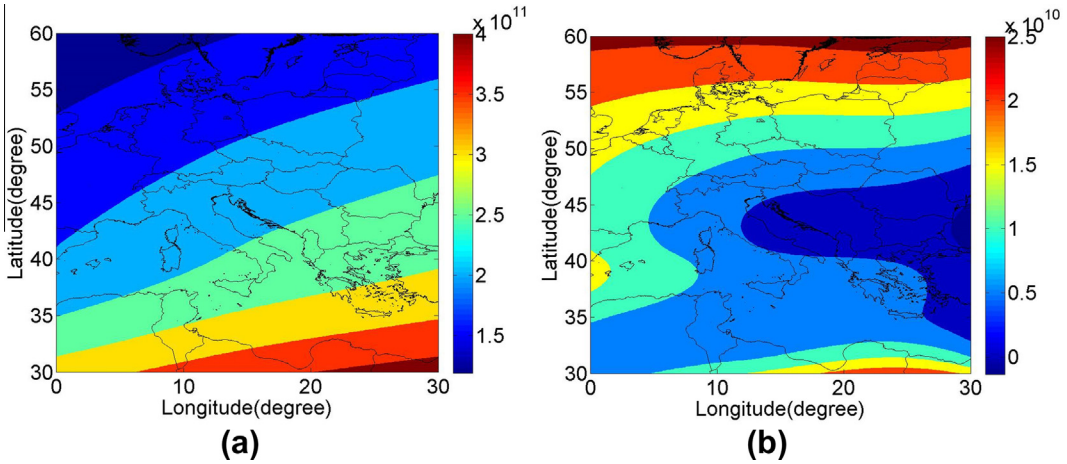

Fig. 15. The distribution of IED for LS-MARS (a) and the error IED between IRI2012 and LS-MARS (b) at heights of 500 km at UT10:00 on DoY61 in 2012, the RMS of the error IED is 3.77E+10 el/m^3.

the maximum electron density occurred 300 km above the surface of the Earth. At various heights, Figs. 10–15 indicate a common feature, indicating that the electron density is large when the latitude is low, reflecting the 3D distribution of electron density in the inversion region.

5. Conclusion

A statistical learning-based method, namely LS-MARS, was proposed in order to estimate the regional 3D IED. MARS was used to automatically select the optimal representing basis functions for the electron density inside that modeling area by using IRI2012 electron density data. Subsequently, this selected basis functions was substituted into the observation equation of the global positioning system total electron content to calculate the design matrix. The weighted damped least squares method was used to reestimate the coefficients of the IED model. Compared with conventional function-based methods, the proposed method can be used to attain optimal model automatically, flexibly, adaptively based on the IRI2012 without a priori knowledge of the IED distribution mathematical function. We tested the proposed method using data from the IGS GPS network on days from DoY60 to DoY61 in 2012 in Europe. The findings showed that the LS-MARS model had smaller recovery TEC error compared with the MARS_IRI2012 model and the VTEC calculated from LS-MARS was more closer to the VTEC obtained from IGS final IONEX files than were the VTEC calculated from the MARS_IRI2012 and IRI2012. Therefore, this method demonstrates strong modeling effectiveness and reliability, it should serve as an attractive and alternative method for estimating regional 3D IED.

References

An, Jiachun., 2011. Ionospheric Tomography Algorithms and their Applications in Polar Area. (Doctoral thesis). University of Wuhan, China.

Austen, J.R., Franke, S.J., Liu, C.H., Yeh, K.C., 1986. Application of computerized tomography techniques to ionospheric research. In: International Beacon Satellite Symposium on Radio Beacon Contribution to the Study of Ionization and Dynamics of the Ionosphere and to Corrections to Geodesy and Technical Workshop, vol. 1, pp. 25–35.

Austen, J.R., Franke, S.J., Liu, C.H., 1988. Ionospheric imaging using computerized tomography. Radio Sci. 23 (3), 299–307.

Brunini, C., Meza, A., Azpilicueta, F., Van Zele, M.A., Gende, M., Díaz, A., 2004. A new ionosphere monitoring technology based on GPS. Astrophys. Space Sci. 290 (3–4), 415–429.

Durmaz, M., Karslioglu, M.O., Nohutcu, M., 2010. Regional VTEC modeling with multivariate adaptive regression splines. Adv. Space Res. 46 (2), 180–189.

Fremouw, E.J., Secan, J.A., Howe, B.M., 1992. Application of stochastic inverse theory to ionospheric tomography. Radio Sci. 27 (5), 721–732.

Friedman, J.H., 1991. Multivariate adaptive regression splines. Ann. Stat. 19 (1), 1–67.

Gao, Y., Liu, Z.Z., 2002. Precise ionosphere modeling using regional GPS network data. Global Position. Syst. 1, 18–24.

Hansen, A., 1998. Real-time ionospheric tomography using terrestrial GPS sensors. In: Proceedings of Ion GPS. Institute of Navigation, vol. 11, pp. 717–728.

Hastie, T., Tibshirani, R., Friedman, J., 2009. The Elements of Statistical Learning: Data Mining, Inference, and Prediction. Springer, New York.

Hernandez-Pajares, M., Juan, J.M., Sanz, J., 1999. New approaches in global ionospheric determination using ground GPS data. J. Atmos. Solar-Terr. Phys. 61 (16), 1237–1247.

Hofmann-Wellenhof, B., Lichtenegger, H., Wasle, E., 2007. GNSS - Global Navigation Satellite Systems: GPS, GLONASS, Galileo, and More. Springer.

Howe, B.M., 1997. 4-D simulations of ionospheric tomography. In: Proceedings of the 1997 National Technical Meeting of the Institute of Navigation, pp. 269–278.

Jekabsons, G., 2010. Areslab: adaptive regression splines toolbox for matlab/octave. Available at <http://www.cs.rtu.lv/jekabsons/>.

Kamp, M.M.J.L., 2013. Medium-scale 4-D ionospheric tomography using a dense GPS network. Ann. Geophys. 31 (1), 75–89.

Koch, K.R., Kusche, J., 2002. Regularization of geopotential determination from satellite data by variance components. J. Geodesy. 76 (5), 259–268.

Kao, S.P., Chen, Y.C., Ning, F.S., 2014. A MARS-based method for estimating regional 2-D ionospheric VTEC and receiver differential code bias. Adv. Space Res. 53 (2), 190–200.

Kunitake, M., Ohtaka, K., Maruyama, T., Tokumaru, M., Morioka, A., Watanabe, S., 1995. Tomographic imaging of the ionosphere over

Japan by the modified truncated SVD method. Ann. Geophys. 13 (12), 1303–1310.

Liu, Z., 2004. Ionosphere Tomography Modeling and Applications Using Global Positioning System (GPS) Measurements (Doctoral thesis). University of Calgary, Canada.

Ma, G., Maruyama, T., 2003. Derivation of TEC and estimation of instrumental biases from GEONET in Japan. Ann. Geophys. 21 (10), 2083–2093.

Rius, A., Ruffini, G., Cucurull, L., 1997. Improving the vertical resolution of ionospheric tomography with GPS occultations. Geophys. Res. Lett. 24 (18), 2291–2294.

Schaer, S., 1999. Mapping and Predicting the Earth's Ionosphere using the Global Positioning System (Doctoral thesis). University of Berne, Switzerland.

Schmidt, M., Bilitza, D., Shum, C.K., Zeilhofer, C., 2008. Regional 4-D modeling of the ionospheric electron density. Adv. Space Res. 42 (4), 782–790.

Wen, D.B., 2007. Investigation of GPS-Based Ionospheric Tomographic Algorithms and their Applications (Doctoral thesis). Chinese Academy of Sciences, China.

Wen, D., Wang, Y., Norman, R., 2012. A new two-step algorithm for ionospheric tomography solution. GPS Solutions 16 (1), 89–94.

Yao, Y., Chen, P., Zhang, S., Chen, J., 2013. A new ionospheric tomography model combining pixel-based and function-based models. Adv. Space Res. 52 (4), 614–621.

Zeilhofer, C., Schmidt, M., Bilitza, D., Shum, C.K., 2009. Regional 4-D modeling of the ionospheric electron density from satellite data and IRI. Adv. Space Res. 43 (11), 1669–1675.

Zou, Y.H., 2004. A Study of Time-Dependent 3-D Ionospheric Tomography with Ground-Based GPS Network and Occultation Observations (Doctoral thesis). University of Wuhan, China.

Zou, Yuhua, Xu, Jisheng, 2003. An algorithm of time-dependent 3-D computerized ionospheric tomography. Chin. J. Radio Sci. 18 (6), 638–643.